Diffusional kurtosis imaging (DKI) incorporation into an intravoxel incoherent motion (IVIM) MR model to measure cerebral hypoperfusion induced by hyperventilation challenge in healthy subjects

Aude Pavilla, Giulio Gambarota, Alessandro Arrigo, Mehdi Mejdoubi, Regis Duvauferrier, Hervé Saint-Jalmes

Diffusional Kurtosis Imaging (DKI) incorporation into Intravoxel Incoherent Motion (IVIM) MR model to measure cerebral hypoperfusion induced by hyperventilation challenge in healthy subjects

Aude Pavilla[1,2,3], Giulio Gambarota[1,2], Alessandro Arrigo,[3] Mehdi Mejdoubi[3], Régis Duvauferrier[3], Hervé Saint-Jalmes[1,2,4]

[1] *INSERM, UMR 1099, Rennes, F-35000, France*

[2] *Université de Rennes 1, LTSI, Rennes, F-35000, France*

[3] *Department of Neuroradiology, Pierre-Zobda-Quitman Hospital, University Hospital of Martinique, French West Indies, France*

[4] *CRLCC, Centre Eugène Marquis, Rennes, F-35000, France*

Corresponding author: Aude Pavilla, MSc

Department of Neuroradiology,Pierre-Zobda-Quitman Hospital,

University Hospital of Martinique, French West Indies.

Tel: +596 596 55 21 81; Fax: +596 596 75 16 68

email: aude.pavilla@gmail.com

Word count of abstract and text: 200 (abstract) ; 3597 (text)

Number of figures and tables: 4 figures and 4 tables

Number of references: 38

Acknowledgments

This study was supported by the Conseil Scientifique et Méthodologique (CSM) of the University Hospital of Martinique (CHU).

Abstract

Object: To investigate the diffusional kurtosis imaging (DKI) incorporation into the intravoxel incoherent motion (IVIM) model for measurements of cerebral hypoperfusion in healthy subjects.

Materials and Methods: Eight healthy subjects underwent a hyperventilation challenge with a four-minute diffusion weighted imaging (DWI) protocol, using 8 b-values chosen with the Cramer-Rao-Lower-Bound optimization approach. Four regions of interest in gray matter (GM) were analyzed with the DKI-IVIM model and the bi-exponential IVIM model, for normoventilation and hyperventilation conditions.

Results: A significant reduction in the perfusion fraction (f) and in the product fD* of the perfusion fraction with the pseudodiffusion coefficient (D*) was found with the DKI-IVIM model, during the hyperventilation challenge. In the cerebellum GM, the percentage changes were f:-43.7±40.1, p=0.011 and fD*:-50.6±32.1, p=0.011; in thalamus GM, f:-47.7±34.7, p=0.012 and fD*:-47.2±48.7, p=0.040. In comparison, using the bi-exponential IVIM model only a significant decrease in the parameter fD* was observed for the same regions of interest. In frontal-GM and posterior-GM, the reduction in f and fD* did not reach statistical significance, either with DKI-IVIM or the bi-exponential IVIM model.

Conclusion: When compared to the bi-exponential IVIM model, the DKI-IVIM model displays a higher sensitivity to detect changes in perfusion induced by the hyperventilation condition.

Keywords: Diffusion magnetic resonance imaging, perfusion, hyperventilation, intravoxel incoherent motion, kurtosis.

Introduction

The IntraVoxel Incoherent Motion (IVIM) is a magnetic resonance imaging (MRI) method that enables for the simultaneous assessment of diffusion and perfusion [1]. In this model [2], the total signal decay obtained by diffusion-weighted imaging (DWI) incorporates a vascular compartment in addition to the pure diffusive compartment (characterized by the diffusion coefficient D). The vascular component arises from the molecules of water in the blood capillaries that mimic a pseudo-diffusion process characterized by the pseudo-diffusion coefficient D*. The perfusion fraction f is another IVIM-derived parameter that represents the capillary vascular volume fraction.

The IVIM method has been applied to several body organs [3–5]; a number of studies on the human brain have also emerged in the last few years. A linear relationship between the perfusion fraction f and the cerebral blood volume (CBV) has been reported [6–8], in particular in gray matter [9].

In the standard IVIM model, here referred to as the "bi-exponential IVIM", the signal decay at different values of diffusion weighting (b-values) can be described with a bi-exponential function. The bi-exponential IVIM model describes the pure diffusive contribution to the total signal decay with a mono-exponential function. However, acquisitions at higher b-values ($b>1000$ s/mm^2) reveals a deviation from a mono-exponential curve [10]. Accordingly, such non-Gaussian effects when the diffusion is restricted/hindered have been investigated with more sophisticated diffusion models, namely, the bi-exponential diffusion model [11, 12], the continuous diffusion compartments [13] or the diffusional kurtosis imaging (DKI) [14]. DKI is based on a mathematical approach that uses a polynomial model with a dimensionless factor called the kurtosis (K). This coefficient is a measure of the deviation from Gaussian behavior and it is often associated with tissue heterogeneity and/or irregularities [15]. The

DKI model has been shown to be robust for parameter quantification and its application has been successfully investigated in previous diffusion studies [16–18]. The incorporation of DKI into the IVIM model (DKI-IVIM model) is of great interest for both perfusion and diffusion characterization. In recent studies, the DKI-IVIM model has been applied to clinical investigations of neck nodal metastases and brain tumours[19, 20]; furthermore, in healthy volunteers, De Luca et al. [21]performed a detailed analysis of the changes of the DKI-IVIM parameters with perfusion, in calf muscle.

In the current study, we sought to investigate whether non-Gaussian diffusion behavior could be identified and quantified by the DKI-IVIM analysis in the specific context of a hyperventilation challenge for perfusion measurements in brain. Specifically, the hyperventilation challenge [22–24] is well known to induce a decrease of cerebral blood volume and blood flow (CBV and CBF, respectively). In a previous study [25], the effects of a similar challenge (which used inhaled gases) on the perfusion fraction f and on the product fD* were investigated with the bi-exponential IVIM model. Thus, in the current study we compared the DKI-IVIM model with the bi-exponential IVIM model in order to identify the most suitable method for detecting perfusion changes, as those that might occur in pathologies such as ischemic stroke. The IVIM-relevant sequence parameters (i.e., the b-values) were optimized using a Cramer-Rao Lower Bound (CRLB) analysis [26], in order to obtain a scan time compatible with clinical examination procedures.

Thus, the overall aim of this study was to assess the ability of the DKI-IVIM model to detect changes in cerebral perfusion in comparison with the standard bi-exponential IVIM model, in a scan time suitable for clinical applications.

Materials and methods

MR imaging

This study was approved by the local institutional review board. Eight healthy volunteers (3 women, 5 men; age 29 ± 4 years) were recruited. MR imaging was performed on a 1.5-T clinical system (Optima MR 450, GE Healthcare, Waukesha, WI, USA) equipped with an eight-channel head coil. Since no specific IVIM protocol for the quantification of cerebral perfusion was provided by the vendor, we designed an optimized IVIM protocol using the vendor-supplied DWI sequence. DWI images were acquired using a single-shot spin-echo echo-planar imaging sequence with the diffusion-weighted gradients (δ/Δ= 36/47 ms) along three orthogonal directions and with the following parameters : ASSET factor = 2, repetition time/echo time (TR/TE) = 3000/75 ms, field of view (FOV) = 250 x 250 mm^2, matrix size = 128 x 128, in-plane resolution = 1.95 x 1.95 mm^2, 27 slices with a slice thickness of 4 mm without gap, bandwidth = 3906 Hz.

A CRLB analysis was performed to determine the optimal set of b-values required to extract, with the best precision: 1) f, D* and D for the bi-exponential IVIM model and 2) f, D*, D and K for the DKI-IVIM model. We introduced for each model a figure of merit that takes into account the standard deviation of each parameter. The figures of merit were written as : $\Gamma_{Bi-exponential\ IVIM} = \frac{\sigma_f}{f} + \frac{\sigma_{D'}}{D'} + \frac{\sigma_D}{D}$ and $\Gamma_{DKI-IVIM} = \frac{\sigma_f}{f} + \frac{\sigma_{D'}}{D'} + \frac{\sigma_D}{D} + \frac{\sigma_K}{K}$ for the bi-exponential IVIM model and the DKI-IVIM model, respectively; $\sigma_f, \sigma_{D'}, \sigma_D, \sigma_K$ are the CRLB computed values while f, D*, D and K represent the target values of these parameters. The minimization procedure of the figure of merit was performed numerically using Mathematica (Wolfram Research Champaign, IL, USA). The target values were chosen in accordance with the literature [27].

Although a minimum of 4 b-values and 5 b-values was required for the bi-exponential IVIM model and the DKI-IVIM model, respectively, this minimum was increased to eight b-values to improve precision, while keeping the scan time suitable for clinical applications. Finally, the optimum b-values set obtained through this procedure was: 0, 60, 80, 300, 400, 900, 1000 and 1500 s/mm^2. The maximum b-value was chosen to ensure adequate SNR for quantification in both grey and white matter [20]. The total acquisition time of the IVIM MR sequence was 4 min. Furthermore, for segmentation purposes T1-weighted anatomical images were acquired with a 3D gradient echo acquisition (TR /TE =10.8/ 4.4 ms, inversion time = 500 ms).

Hyperventilation challenge

The first IVIM measurement was performed while the subject breathed normally (normoventilation condition, NV). Then, the hypocapnia condition was achieved through hyperventilation, with the aid of metronome beeps played over the headphones to pace the subject's breathing twice as fast as in NV condition [28]. During this hyperventilation challenge, the CO_2 respiratory levels and the ventilation rate were continuously monitored using a nasal cannula; a gas sampler/analyzer displayed the end-tidal partial pressure of CO_2 ($P_{ET}CO_2$) in mmHg and the ventilation rate in breaths per minute. Once the subject was in a stationary condition (hyperventilation condition, HV), a second IVIM measurement was performed. The $P_{ET}CO_2$ and ventilation rate were measured each minute during the IVIM acquisitions in both NV and HV conditions, to ensure the efficiency of the hyperventilation challenge. Values of $P_{ET}CO_2$ were used as an indirect measure of the arterial partial pressure of CO_2 (P_aCO_2).

Image Processing

MR images were transferred to an independent workstation for post-processing. For each subject, the T1-weighted anatomical images were voxel-wise segmented into to gray matter (GM), white matter (WM), and cerebrospinal fluid (CSF) probability maps using the FAST (FMRIB's Automated Segmentation Tool) tool in FSL (FMRIB Software Library, Oxford, UK). A gray matter mask was created at a threshold of 0.9 to mitigate partial volume effect with WM and CSF. The diffusion-weighted images in NV conditions and the gray matter mask were first co-registered together. Four regions of interest (ROIs) were drawn in the cerebellum GM, the thalamus GM, the frontal GM and the posterior GM. Then, the same co-registration procedure was applied to diffusion-weighted images in HV condition and the four ROIs were copied to these images for subsequent comparison and analysis.

The IVIM analysis was subsequently performed with in-house MATLAB scripts (MATLAB 2016a, MathWorks, Natick, MA, USA) based on the nonlinear least-square fitting method with the Trust-Region algorithm.

The bi-exponential function in the conventional IVIM model is given by the expression :

$$\frac{S(b)}{S_0} = f e^{-bD^*} + (1-f)e^{-bD} \quad [1]$$

where S(b) and S_0 are the signal obtained with and without (b=0s/mm^2) diffusion encoding, respectively.

The DKI-IVIM model is described by the equation :

$$\frac{S(b)}{S_0} = f e^{-bD^*} + (1-f)e^{-bD+\frac{b^2D^2K}{6}} \quad [2]$$

where K is the Kurtosis factor that quantifies the deviation from the Gaussian behavior. K=0 corresponds to the case of Gaussian diffusion.

The direct fitting method that estimates all IVIM parameters simultaneously has been shown to provide limited reliability and precision due to limited number of samples, noise and non-linearity as reported in other IVIM studies [4, 29]. For this reason, a "segmented" technique considering the diffusion signal at high and low b-values separately was used to analyze the IVIM data [30, 31]. The segmented algorithm consisted of three steps. First, since D* is significantly greater than D, the effect of D* on the signal can be considered negligible when b-values are large enough (typically, for b-values greater than 300 s/mm^2). Thus D and K were obtained by fitting the signal (b-values > 300 s/mm^2) to the function:

$$\frac{S(b > 300)}{S_0} = \frac{S_{Int}}{S_0} e^{-bD} \quad [3]$$

for the bi-exponential IVIM model, and to the function:

$$\frac{S(b > 300)}{S_0} = \frac{S_{Int}}{S_0} e^{-bD+\frac{b^2D^2K}{6}} \quad [4]$$

for the DKI-IVIM model.

In both cases, $\frac{S_{Int}}{S_0}$ is the intercept of the normalized diffusion-related signal (b > 300 s/mm^2) with the y-axis (in other terms, the normalized value of the signal at b = 0 s/mm^2 if no pseudo-diffusion component was present). In the second step, for both models the perfusion fraction was computed as: $f = 1 - \frac{S_{Int}}{S_0}$. Finally, the Trust-Region algorithm was used to determine the value of the pseudo diffusion coefficient D* based on Eq. [1] for bi-exponential IVIM model and Eq. [2] for DKI-IVIM model, using all data points and the values determined for D (D and K, for DKI-IVIM model) and f. The parameter fD*, which has been associated to the blood-flow [8], was obtained by scalar multiplication.

For non-physiologically acceptable values of f (close to 1), that may reflects undetectable perfusion (vascular component vanishing), the perfusion fraction was set to zero while D* was not defined.

Data analysis and statistical analysis

In order to compare the curve fitting results obtained with the bi-exponential IVIM and DKI-IVIM models, the Akaike Information Criterion (AIC) was used [32]:

$$AIC = N\ln(SS) + 2k \quad [5]$$

where N is the sample size (number of points), SS is the sum of squared deviations and k the number of estimated parameters. The formula of the AIC value shows that the Akaike information criterion takes into account the goodness of the fit as well as the complexity of the model. The model with the lower AIC value is the preferred model. Therefore, for a given fit, the AIC difference between the two models was computed as follows: $\Delta AIC = AIC(Biexponential) - AIC(DKI)$; given the above definition, a positive ΔAIC value indicates that the DKI-IVIM model is preferred over the bi-exponential IVIM; whereas a negative ΔAIC value indicates that the bi-exponential IVIM model is preferred over the DKI-IVIM model.

A paired Student t-test was performed to determine the statistical differences between NV and HV conditions for all the estimated IVIM parameters with both IVIM models. A significant level of 0.05 was adopted.

Results

The efficiency of the hyperventilation challenge was validated by a significant decrease of the end-tidal partial pressure of CO_2 ($P_{ET}CO_2$), from the normoventilation to the hyperventilation condition ($p < 0.0001$). **Figure 1** shows the $P_{ET}CO_2$ levels during the IVIM protocol in both conditions. It is also noteworthy that the $P_{ET}CO_2$ levels remained stable during both IVIM measurements.

Figure 2 shows an example of axial IVIM images (b = 80 s/mm^2) in one volunteer (subject no. 5 in **Table 3** and **Table 4:** male, 35 years old) with the ROIs in the cerebellum GM, thalamus GM, posterior and frontal GM. In **Figure 3**, the plot of the signal intensity as a function of the b-values from the same volunteer, for the thalamus GM ROI under normoventilation (NV) and hyperventilation (HV), is presented. The bi-exponential IVIM (**Figure 3a**) and DKI-IVIM (**Figure 3b**) curve fit is represented by the solid lines, for each ventilatory condition. The effect of the hyperventilation challenge on the perfusion can be revealed by visual inspection. Indeed, while the slope between b = 300 s/mm^2 and b = 1500 s/mm^2, which is proportional to the diffusion coefficient D, did not differ between NV and HV conditions, the slope between b = 0 s/mm^2 and b = 300 s/mm^2, which is proportional to the blood-flow related IVIM parameter fD*, decreased under HV condition with both IVIM models. Moreover, the y-intercept of the line fitted between b = 300 s/mm^2 and b = 1500 s/mm^2 was higher for the HV condition; this means that the perfusion fraction f in the HV condition was smaller than in the NV condition, as expected during a hyperventilation challenge, where the cerebral blood volume and flow are reduced. This observation was common to the two IVIM models investigated. On the other hand, when looking closer at the curve fit of the signal between b = 300 s/mm^2 and b = 1500 s/mm^2, in **Figure 3c** and **3d,** a slight tendency to a better fit with the DKI-IVIM model for high b-values, at least in NV

condition could be noted. These findings were further supported by the analysis based on Aïkake Information Criterion, which showed that the DKI-IVIM model was the more appropriate model to fit the data for both ventilatory conditions. As a matter of fact, the value ΔAIC (averaged over all ROIs, in both ventilatory conditions and for all volunteers) was significantly greater than zero ($p < 0.0001$).

The changes in the IVIM parameters induced by the hyperventilation were estimated using the two models. The statistics of the changes in the perfusion parameters f and fD*, averaged over all volunteers in the four ROIs, is summarized in **Table 1**. **Table 2** summarizes the changes in the diffusion parameters D and K. We observed a reduction of f and fD* when the volunteers hyperventilated, with both the bi-exponential IVIM and the DKI-IVIM model, in the cerebellum and thalamus GM ROIs. Concerning the perfusion fraction f, the differences were most statistically significant with a - 43.7% change in the cerebellum GM ($p = 0.011$) and a - 47.7 % change in the thalamus GM ($p = 0.012$), with the DKI-IVIM model, as also shown in **Figure 4**. The blood-flow related IVIM parameter fD* significantly decreased in the cerebellum GM and thalamus GM ROIs, as assessed by the bi-exponential IVIM analysis. The DKI-IVIM model led to the same conclusion but displayed a higher sensitivity, in comparison to the bi-exponential IVIM model, to detect changes in fD* for those two ROIs. On the other hand, in frontal and posterior GM, the reduction in f and fD* did not reach statistical significance, either with DKI-IVIM or the bi-exponential IVIM model. An abnormal increase in fD* was observed with the bi-exponential IVIM model in posterior GM.

No significant changes in the diffusion parameters D and K (DKI-IVIM model) and D (bi-exponential IVIM) were observed during the hyperventilation challenge, with the exception of the frontal GM that exhibited a slight significant increase.

Table 3 shows the changes in f and fD* for each volunteer in the cerebellum ROI, chosen here as an example. A decrease of the perfusion parameters f and fD* was observed with the

DKI-IVIM model in all volunteers, with the exception of the volunteer no. 4. The bi-exponential IVIM model yielded a decrease of f and fD* in all volunteers but no. 1, 4 and 5. Furthermore, the decrease observed in f and fD* with the bi-exponential IVIM model was substantially smaller than that observed with the DKI-IVIM model. In **Table 4**, the changes in D and K, induced by the hyperventilation challenge, are shown for each volunteer in the cerebellum ROI. The changes in D and K were much smaller than the changes observed in f and fD*, with the majority of the changes (in D and K) being less than 10%.

Discussion

In the current study, IVIM diffusion decays were acquired in eight healthy volunteers in normo- and hyper-ventilation conditions; this latter condition is known to induce cerebral hypoperfusion, thus mimicking a physiological event that might occur in a number of pathologies. Two models were investigated to analyze the IVIM diffusion decays: the "standard" bi-exponential IVIM model and the DKI-IVIM model. The DKI-IVIM model appeared to be the better model, based on the Aïkake Information Criterion and on the higher sensitivity to detect the changes in perfusion induced by the hyperventilation condition.

A significant reduction in both f and fD* was found with the DKI-IVIM model during the hyperventilation challenge in the cerebellum and thalamus GM ROIs. A trend toward reduction of f and fD* for the frontal and posterior GM ROIs was also observed.

In comparison, using the bi-exponential IVIM model, only a significant decrease in fD* was observed in the cerebellum and thalamus GM ROIs. In posterior GM, the abnormal increase in fD* could be due to partial volume confounding effects, arising from both white matter and cerebro-spinal fluid contamination. In general, it is noteworthy that the frontal and posterior GM ROIs exhibit moderate-to-severe confounding effects of partial volume, despite the segmentation procedure, due to their location. Averaged over all volunteers, the perfusion parameters estimated in these ROIs showed a larger variance, compared to the cerebellum and the thalamus; similar observations were also reported in a previous study [25].

The bi-exponential IVIM model allows for the simultaneous quantification of the water diffusion and of the perfusion in the capillary microcirculation. With respect to the water diffusion, this model does not consider the non-Gaussian behavior related to restricted/hindered diffusion, which might play an important role at higher b-values. The DKI model is one of the alternate models that addresses this non-Gaussian behavior of water

diffusion [14]; it has been widely explored this last decade providing encouraging results for improved tissue characterization [16–18]. However, the DKI method implementation and its extension to IVIM requires inevitably longer scan times to acquire data at higher b-values and with enough SNR; furthermore, in comparison to the bi-exponential approach, the DKI-IVIM model adds an another degree of freedom to the nonlinear least-squares fitting, that is already SNR demanding. For these reasons, probably, widespread clinical applications of DKI have been so far limited [15–18, 20]. On the other hand, DKI-IVIM has the advantage to provide an estimation of the kurtosis factor (K), which might represent a potential complementary biomarker of tissue diffusivity.

The kurtosis factor K could be of interest for clinical applications, as preliminary studies report in oncology [19, 33]. K is a phenomenological index that does not have a direct biophysical interpretation but can be correlated indirectly to biophysical processes or indexes. It has been hypothesized that the kurtosis factor at least might reflect the interaction of water molecules with cell membranes and intracellular components [34, 35]. The DKI-IVIM incorporates the non- Gaussian DKI diffusion model into IVIM imaging, and thus it provides a measure of water diffusion, perfusion and kurtosis in a given tissue.

The application of DKI-IVIM in clinical settings requires short scan times; to this aim, it is crucial to optimize the pulse sequence parameters. In the current study, an optimized IVIM protocol was developed using the CRLB approach to identify the optimal b-values for improved precision on the parameters D, f, D* and K. Eight b-values ranging from 0 to 1500 s/mm^2 were used, for a total scan time of four minutes. The study protocol included an hyperventilation challenge. This challenge is well known to induce a reduction in cerebral perfusion associated with hypocapnia conditions [22, 28] characterized by simultaneous CBV and CBF decrease. The use of this challenge allows for mimicking a perfusion impairment similar to that occurs in ischemic stroke, for instance. The end-tidal partial pressure of CO_2

($P_{ET}CO_2$) was monitored during the challenge to corroborate that the physiologic effects of hypocapnia was indeed taking place during the IVIM acquisitions. On the other hand, no significant correlation was found between the perfusion parameters and the difference of $P_{ET}CO_2$. This could probably be ascribed to the small cohort size (n = 8).

In the IVIM model, the parameter f reflects the capillary blood volume fraction and the parameter fD* represents an index proportional to the capillary blood flow; indeed, a correlation between f and CBV measured by dynamic susceptibility contrast (DSC-MRI) has been reported in brain gray matter [9] and gliomas [20]; the fD* has been shown to be a sensitive metric to quantify cerebral blood flow [36, 37]. Furthermore, theoretical relationships between f and CBV and between fD* and CBF were proposed [6] but they require the knowledge of the capillary geometry, which is likely to vary with anatomy and pathologies; overall, these theoretical relationships remain still object of debate [9, 38]. In the current study, a decrease in both f an fD* (with the DKI-IVIM model) was observed during the hyperventilation challenge; thus, the results of our work corroborate the idea that IVIM-derived parameters f and fD* are valid physiological markers of perfusion; as such, they are of interest in investigations of pathologies that affect the status of the capillary network.

This study suffers from some limitations. The number of subjects was small. Furthermore, the maximum value of the b-factor was limited to 1500 s/mm^2, which may not be the optimal value, according to kurtosis non-Gaussian theory. Another limitation of the current study is that the data analysis was performed on regions of interest rather than on a voxel-by-voxel basis. In the supplementary materials, parametric maps of f and fD* are shown.The quality of these maps needs to be improved; to estimate the IVIM parameters on a voxel-by-voxel fashion, it will be necessary to increase the number of acquired b-values and/or the number of averages, at the expense of increasing the scan time. Another possible option would be to perform the measurements on a 3T MR system, which will ensure a higher SNR.

Compliance with Ethical Standards

Disclosure of potential conflicts of interest

The authors each declare that they have no conflict of interest.

Research involving Human Participants and/or Animals

All procedures performed in studies involving human participants were approved by the appropriate ethics committee and were therefore performed in accordance with the ethical standards laid down in the 1964 Declaration of Helsinki and its later amendments.

Informed consent

Informed consent was obtained from all individual participants included in the study.

Authors' Contribution

Pavilla: Protocol/ Data collection / Data analysis

Gambarota: Protocol/ Data analysis/ project development

Arrigo: Protocol/ Data collection management/ project development

Mejdoubi: Protocol/project development

Duvauferrier: Protocol/project development

Saint-Jalmes:Protocol /Data analysis/ project development

References

1. Le Bihan D, Breton E, Lallemand D, Grenier P, Cabanis E, Laval-Jeantet M (1986) MR imaging of intravoxel incoherent motions: application to diffusion and perfusion in neurologic disorders. Radiology 161:401–407.

2. Le Bihan D, Breton E, Lallemand D, Aubin ML, Vignaud J, Laval-Jeantet M (1988) Separation of diffusion and perfusion in intravoxel incoherent motion MR imaging. Radiology 168:497–505.

3. Koh D-M, Collins DJ, Orton MR (2011) Intravoxel incoherent motion in body diffusion-weighted MRI: reality and challenges. AJR Am J Roentgenol 196:1351–1361.

4. Luciani A, Vignaud A, Cavet M, Nhieu JTV, Mallat A, Ruel L, Laurent A, Deux J-F, Brugieres P, Rahmouni A (2008) Liver cirrhosis: intravoxel incoherent motion MR imaging--pilot study. Radiology 249:891–899.

5. Le Bihan D (2008) Intravoxel Incoherent Motion Perfusion MR Imaging: A Wake-Up Call [1]. Radiology 249:748–752.

6. Le Bihan D, Turner R (1992) The capillary network: a link between IVIM and classical perfusion. Magn Reson Med 27:171–178.

7. Wirestam R, Borg M, Brockstedt S, Lindgren A, Holtås S, Ståhlberg F (2001) Perfusion-related parameters in intravoxel incoherent motion MR imaging compared with CBV and CBF measured by dynamic susceptibility-contrast MR technique. Acta Radiol Stockh Swed 1987 42:123–128.

8. Federau C, O'Brien K, Meuli R, Hagmann P, Maeder P (2014) Measuring brain perfusion with intravoxel incoherent motion (IVIM): Initial clinical experience: Brain IVIM: Initial Clinical Experience. J Magn Reson Imaging 39:624–632.

9. Wu W-C, Chen Y-F, Tseng H-M, Yang S-C, My P-C (2015) Caveat of measuring perfusion indexes using intravoxel incoherent motion magnetic resonance imaging in the human brain. Eur Radiol 25:2485–2492.

10. Mulkern RV, Haker SJ, Maier SE (2009) On high b diffusion imaging in the human brain: ruminations and experimental insights. Magn Reson Imaging 27:1151–1162.

11. Clark CA, Le Bihan D (2000) Water diffusion compartmentation and anisotropy at high b values in the human brain. Magn Reson Med 44:852–859.

12. Sehy JV, Ackerman JJH, Neil JJ (2002) Evidence that both fast and slow water ADC components arise from intracellular space. Magn Reson Med 48:765–770.

13. Bennett KM, Schmainda KM, Bennett (Tong) R, Rowe DB, Lu H, Hyde JS (2003) Characterization of continuously distributed cortical water diffusion rates with a stretched-exponential model. Magn Reson Med 50:727–734.

14. Jensen JH, Helpern JA (2010) MRI quantification of non-Gaussian water diffusion by kurtosis analysis. NMR Biomed 23:698–710.

15. Rosenkrantz AB, Padhani AR, Chenevert TL, Koh D-M, De Keyzer F, Taouli B, Le Bihan D (2015) Body diffusion kurtosis imaging: Basic principles, applications, and considerations for clinical practice: Body Diffusion Kurtosis Imaging. J Magn Reson Imaging 42:1190–1202.

16. Weber RA, Hui ES, Jensen JH, Nie X, Falangola MF, Helpern JA, Adkins DL (2015) Diffusional Kurtosis and Diffusion Tensor Imaging Reveal Different Time-Sensitive Stroke-Induced Microstructural Changes. Stroke 46:545–550.

17. Zhu J, Zhuo C, Qin W, Wang D, Ma X, Zhou Y, Yu C (2015) Performances of diffusion kurtosis imaging and diffusion tensor imaging in detecting white matter abnormality in schizophrenia. NeuroImage Clin 7:170–176.

18. Bai Y, Lin Y, Tian J, Shi D, Cheng J, Haacke EM, Hong X, Ma B, Zhou J, Wang M

(2016) Grading of Gliomas by Using Monoexponential, Biexponential, and Stretched Exponential Diffusion-weighted MR Imaging and Diffusion Kurtosis MR Imaging. Radiology 278:496–504.

19. Lu Y, Jansen JFA, Mazaheri Y, Stambuk HE, Koutcher JA, Shukla-Dave A (2012) Extension of the intravoxel incoherent motion model to non-gaussian diffusion in head and neck cancer. J Magn Reson Imaging 36:1088–1096.

20. Wu W-C, Yang S-C, Chen Y-F, Tseng H-M, My P-C (2016) Simultaneous assessment of cerebral blood volume and diffusion heterogeneity using hybrid IVIM and DK MR imaging: initial experience with brain tumors. Eur Radiol. doi: 10.1007/s00330-016-4272-z

21. De Luca A, Bertoldo A, Froeling M (2016) Effects of perfusion on DTI and DKI estimates in the skeletal muscle: Effects of Perfusion on DTI and DKI in Muscle. Magn Reson Med. doi: 10.1002/mrm.26373

22. Kety SS, Schmidt CF (1946) The effects of active and passive hyperventilation on cerebral blood flow, cerebral oxygen consumption, cardiac output, and blood pressure of normal young men. J Clin Invest 25:107–119.

23. Moreton FC, Dani KA, Goutcher C, O'Hare K, Muir KW (2016) Respiratory challenge MRI: Practical aspects. NeuroImage Clin 11:667–677.

24. Zhang J, Zhou D, Nguyen TD, Spincemaille P, Gupta A, Wang Y (2016) Cerebral metabolic rate of oxygen ($CMRO_2$) mapping with hyperventilation challenge using quantitative susceptibility mapping (QSM). Magn Reson Med. doi: 10.1002/mrm.26253

25. Federau C, Maeder P, O'Brien K, Browaeys P, Meuli R, Hagmann P (2012) Quantitative Measurement of Brain Perfusion with Intravoxel Incoherent Motion MR Imaging. Radiology 265:874–881.

26. Leporq B, Saint-Jalmes H, Rabrait C, Pilleul F, Guillaud O, Dumortier J, Scoazec J-Y, Beuf O (2015) Optimization of intra-voxel incoherent motion imaging at 3.0 Tesla for fast

liver examination: Optimization of Liver Motion Imaging at 3.0T. J Magn Reson Imaging 41:1209–1217.

27. Federau C, Sumer S, Becce F, Maeder P, O'Brien K, Meuli R, Wintermark M (2014) Intravoxel incoherent motion perfusion imaging in acute stroke: initial clinical experience. Neuroradiology 56:629–635.

28. Tancredi FB, Hoge RD (2013) Comparison of cerebral vascular reactivity measures obtained using breath-holding and CO2 inhalation. J Cereb Blood Flow Metab 33:1066–1074.

29. Suo S, Cao M, Zhu W, Li L, Li J, Shen F, Zu J, Zhou Z, Zhuang Z, Qu J, Chen Z, Xu J (2016) Stroke assessment with intravoxel incoherent motion diffusion-weighted MRI: Ivim Diffusion-Weighted Mri for Human Stroke. NMR Biomed 29:320–328.

30. Suo S, Lin N, Wang H, Zhang L, Wang R, Zhang S, Hua J, Xu J (2015) Intravoxel incoherent motion diffusion-weighted MR imaging of breast cancer at 3.0 tesla: Comparison of different curve-fitting methods: Different IVIM Analyses in Breast Cancer. J Magn Reson Imaging 42:362–370.

31. Barbieri S, Donati OF, Froehlich JM, Thoeny HC (2016) Impact of the calculation algorithm on biexponential fitting of diffusion-weighted MRI in upper abdominal organs. Magn Reson Med 75:2175–2184.

32. Akaike H (1974) A new look at the statistical model identification. IEEE Trans Autom Control 19:716–723.

33. Yuan J, Yeung DKW, Mok GSP, Bhatia KS, Wang Y-XJ, Ahuja AT, King AD (2014) Non-Gaussian Analysis of Diffusion Weighted Imaging in Head and Neck at 3T: A Pilot Study in Patients with Nasopharyngeal Carcinoma. PLoS ONE 9:e87024.

34. Le Bihan D (2013) Apparent Diffusion Coefficient and Beyond: What Diffusion MR Imaging Can Tell Us about Tissue Structure. Radiology 268:318–322.

35. Grinberg F, Farrher E, Ciobanu L, Geffroy F, Le Bihan D, Shah NJ (2014) Non-Gaussian

Diffusion Imaging for Enhanced Contrast of Brain Tissue Affected by Ischemic Stroke. PLoS ONE 9:e89225.

36. Federau C, Meuli R, O'Brien K, Maeder P, Hagmann P (2014) Perfusion Measurement in Brain Gliomas with Intravoxel Incoherent Motion MRI. Am J Neuroradiol 35:256–262.

37. Federau C, O'Brien K, Birbaumer A, Meuli R, Hagmann P, Maeder P (2015) Functional Mapping of the Human Visual Cortex with Intravoxel Incoherent Motion MRI. PLOS ONE 10:e0117706.

38. Bisdas S, Braun C, Skardelly M, Schittenhelm J, Teo TH, Thng CH, Klose U, Koh TS (2014) Correlative assessment of tumor microcirculation using contrast-enhanced perfusion MRI and intravoxel incoherent motion diffusion-weighted MRI: is there a link between them?. NMR Biomed 27:1184–1191.

Figures

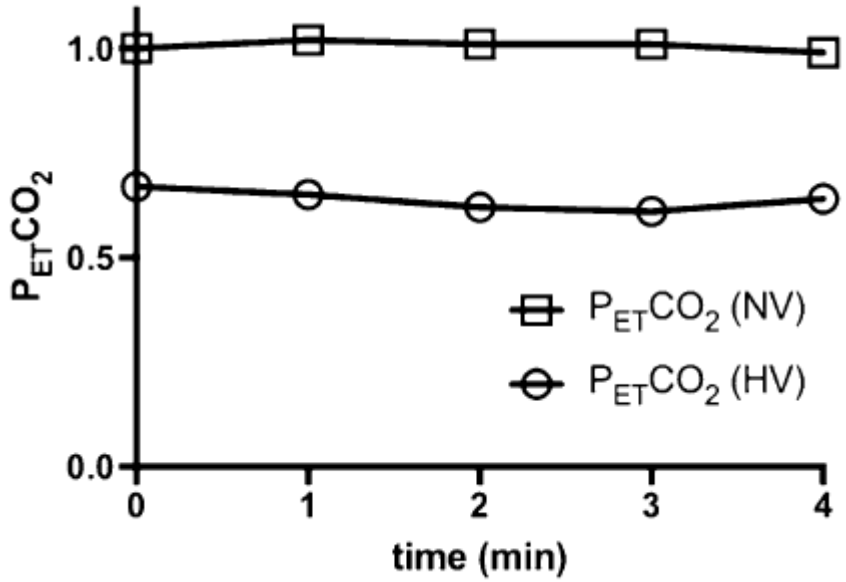

Fig. 1 $P_{ET}CO_2$ time evolution at rest and during the hyperventilation challenge.

Normalized $P_{ET}CO_2$ time course (in minutes) averaged over all subjects each minute during IVIM acquisition. For normoventilation (NV) conditions, $P_{ET}CO_2$ data were normalized to the initial values; for hyperventilation (HV) conditions, $P_{ET}CO_2$ values were normalized to the NV values at the same time point. These time courses show, first, that the $P_{ET}CO_2$ is approximately constant over the sequence duration and second, that there is a significant decrease of $P_{ET}CO_2$ during the hyperventilation challenge.

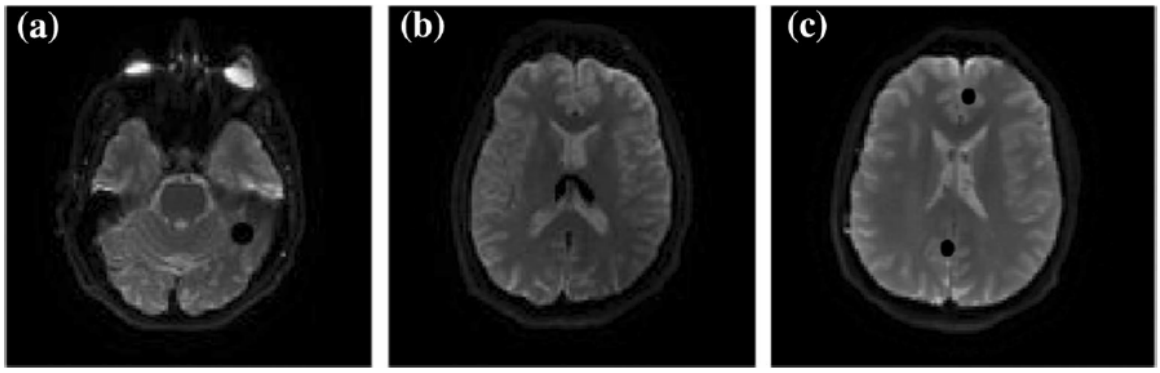

Fig. 2 ROI delineation

Example of ROI delineation on one single slice of diffusion-weighted images (b = 80 s/mm^2) in the same subject. The free-hand ROI in cerebellum (a), thalamus (b) , posterior and frontal (c) GM is depicted in black.

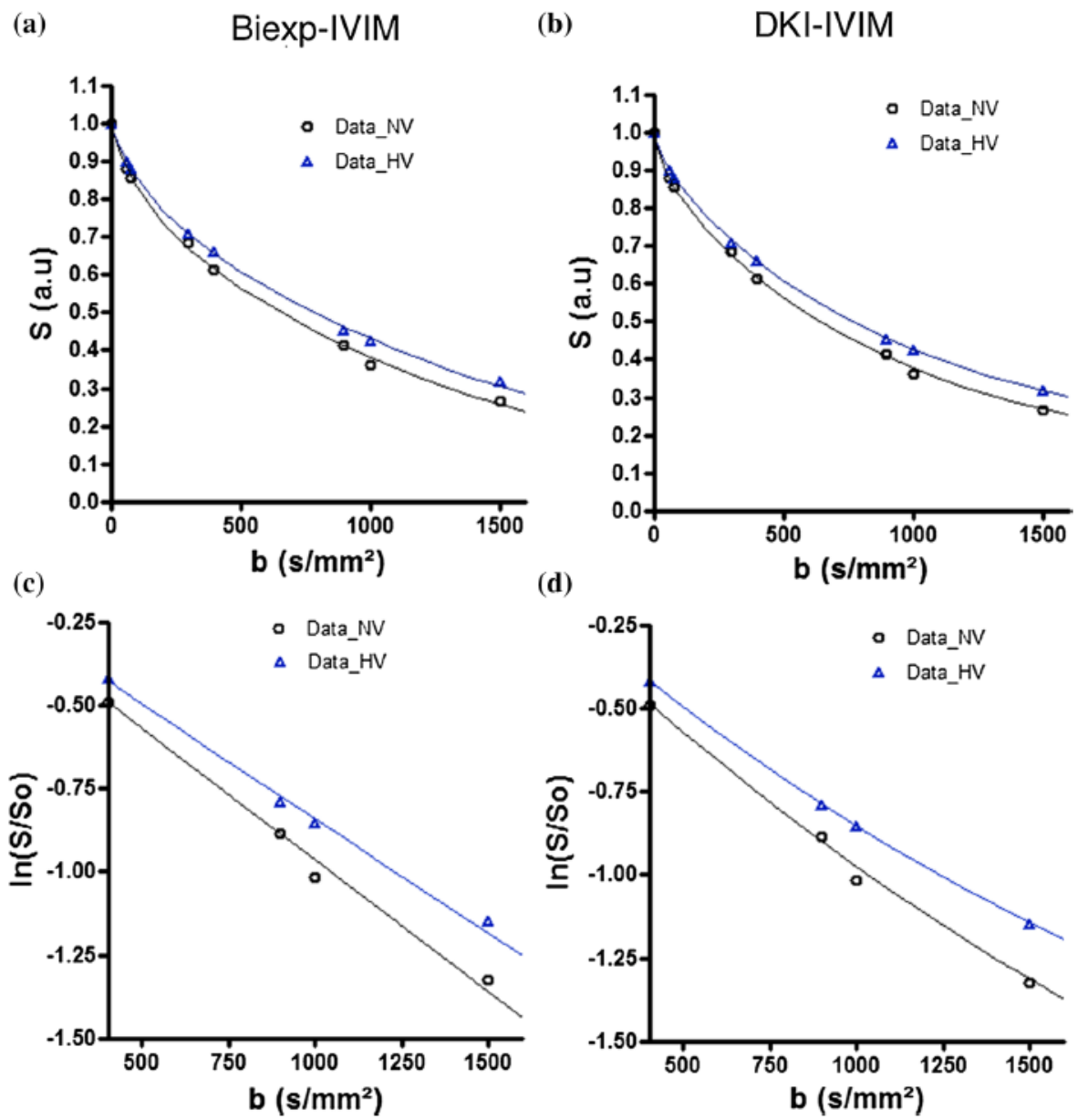

Fig. 3 Example of IVIM analysis on the thalamus ROI

(a) An example of the IVIM signal decay in thalamus GM and the curve fitting with the bi-exponential IVIM (Biexp-IVIM) model, under normoventilation (NV) and hyperventilation (HV) conditions. The slope between b = 0 s/mm^2 and b = 300 s/mm^2, which represents an estimate of the blood flow related IVIM fD* parameter, decreased during the hyperventilation condition.

(b) The same IVIM signal decay in thalamus GM as in (a), with DKI-IVIM curve fitting.

(c) Zoom-in of (a), for b-values between b = 300 s/mm^2 and b = 1500 s/mm^2 , plotted on

logarithmic scale.

(d) Zoom-in of (b), for b-values between b = 300 s/mm^2 and b = 1500 s/mm^2 , plotted on logarithmic scale. The DKI-IVIM model appears to provide a better fit to the data, at least in NV condition, when compared to the Biexp-IVIM model (c)

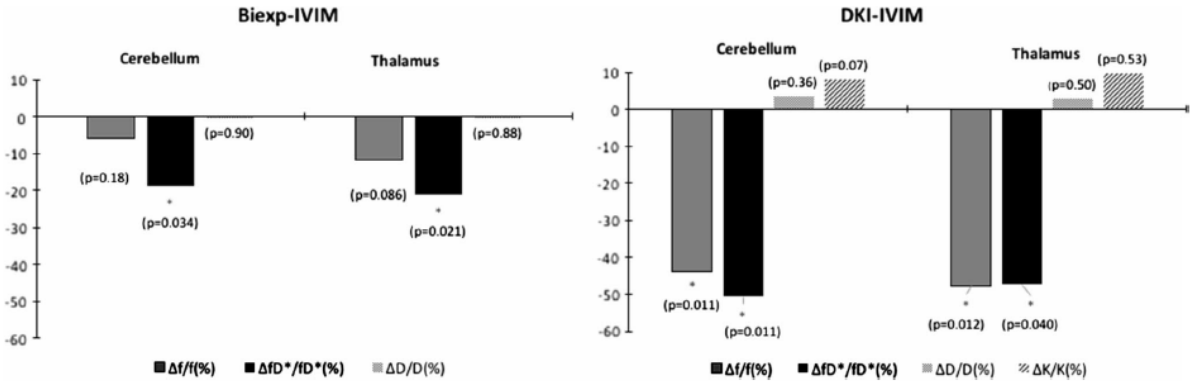

Fig. 4 Normalized percent changes during the hyperventilation challenge.

Normalized percent changes for the perfusion and diffusion IVIM parameters averaged over all volunteers during the hyperventilation challenge. For each model, a paired Student t -test (level of significance $p<0.05$) was performed

Tables

	Model	f_NV	$\Delta(f)/f$ (%)	fD^*_NV	$\Delta(fD^*)/fD^*$ (%)
Cerebellum GM	Biexp-IVIM	0.11 ± 0.04	−5.8 ± 25.1 ($p = 0.18$)	0.07 ± 0.04	−18.8 ± 30.1* ($p = 0.034$)
	DKI–IVIM	0.06 ± 0.03	−43.7 ± 40.1* ($p = 0.011$)	0.05 ± 0.03	−50.6 ± 32.1* ($p = 0.011$)
Thalamus GM	Biexp-IVIM	0.11 ± 0.03	−11.7 ± 16.9 ($p = 0.086$)	0.10 ± 0.04	−21.1 ± 20.0* ($p = 0.021$)
	DKI–IVIM	0.06 ± 0.02	−47.7 ± 34.7* ($p = 0.012$)	0.10 ± 0.06	−47.2 ± 48.7* ($p = 0.040$)
Posterior GM	Biexp-IVIM	0.11 ± 0.04	−13.0 ± 27.1 ($p = 0.21$)	0.07 ± 0.03	22.8 ± 22.8* ($p = 0.035$)
	DKI–IVIM	0.05 ± 0.03	−30.4 ± 65.5 ($p = 0.72$)	0.04 ± 0.02	−43.05 ± 54.5 ($p = 0.14$)
Frontal GM	Biexp-IVIM	0.10 ± 0.02	1.64 ± 31.8 ($p = 0.95$)	0.08 ± 0.02	5.7 ± 50.6 ($p = 0.89$)
	DKI–IVIM	0.06 ± 0.03	−34.2 ± 43.6 ($p = 0.095$)	0.07 ± 0.03	−22.3 ± 69.3 ($p = 0.73$)

Baseline [in normoventilation (NV) condition] values and normalized percent changes averaged over all the volunteers during the hyperventilation challenge are reported. The results are expressed as mean ± standard deviation

Asterisks indicate any significant changes during the hyperventilation challenge ($p < 0.05$)

Table 1. Summary of the statistics of the perfusion parameters f and fD* ($x10^{-2}$ mm^2/s) obtained with the bi-exponential IVIM and DKI-IVIM models. Baseline (in normoventilation (NV) condition) values and normalized percent changes averaged over all the volunteers during the hyperventilation challenge are reported. The results are expressed as mean ± standard deviation.

	Model	D_NV	$\Delta(D)/D$ (%)	K_NV	$\Delta(K)/K$ (%)
Cerebellum GM	Biexp-IVIM	0.56 ± 0.05	-0.19 ± 4.74 ($p = 0.89$)	–	–
	DKI–IVIM	0.87 ± 0.07	2.9 ± 9.2 ($p = 0.36$)	0.74 ± 0.16	9.0 ± 28 ($p = 0.07$)
Thalamus GM	Biexp-IVIM	0.72 ± 0.03	-0.15 ± 5.8 ($p = 0.88$)	–	–
	DKI–IVIM	0.91 ± 0.07	3.2 ± 16 ($p = 0.50$)	0.62 ± 0.14	-3.8 ± 55 ($p = 0.53$)
Posterior GM	Biexp-IVIM	0.74 ± 0.07	-1.6 ± 6.4 ($p = 0.42$)	–	–
	DKI–IVIM	0.92 ± 0.12	-0.35 ± 11 ($p = 0.78$)	0.78 ± 0.19	0.69 ± 19 ($p = 0.65$)
Frontal GM	Biexp-IVIM	0.81 ± 0.04	6.3 ± 6.0* ($p = 0.02$)	–	–
	DKI–IVIM	0.93 ± 0.05	11.3 ± 8.6* ($p = 0.01$)	0.50 ± 0.13	16.5 ± 21.2* ($p = 0.03$)

Baseline [in normoventilation (NV) condition] values and normalized percent changes averaged over all the volunteers during the hyperventilation challenge are reported. The results are expressed as mean ± standard deviation

Asterisks indicate any significant changes during the hyperventilation challenge ($p < 0.05$)

Table 2. Summary of the statistics of the diffusion parameters D ($x10^{-3}$ mm^2/s) and K obtained with the bi-exponential IVIM and DKI-IVIM models. Baseline (in normoventilation (NV) condition) values and normalized percent changes averaged over all the volunteers during the hyperventilation challenge are reported. The results are expressed as mean ± standard deviation.

Volunteer no.	Model	$\Delta f/f$ (%)	$\Delta fD^*/fD^*$ (%)
1	Biexp-IVIM	45.8	40.4
	DKI–IVIM	−90.3	−99.9
2	Biexp-IVIM	−21.4	−39.0
	DKI–IVIM	−37.3	−54.8
3	Biexp-IVIM	−37.9	−45.2
	DKI–IVIM	−66.7	−73.2
4	Biexp-IVIM	9.1	14.4
	DKI–IVIM	37.5	10.7
5	Biexp-IVIM	0.0	−39.4
	DKI–IVIM	−36.1	−65.0
6	Biexp-IVIM	−17.6	−27.6
	DKI–IVIM	−71.8	−36.8
7	Biexp-IVIM	−11.1	−27.9
	DKI–IVIM	−19.2	−43.4
8	Biexp-IVIM	−13.4	−26.3
	DKI–IVIM	−65.1	−42.3

Table 3. Individual normalized percent changes of the IVIM perfusion parameters f and fD* obtained with the bi-exponential IVIM and DKI-IVIM models in the cerebellum gray matter ROI, from the 8 healthy volunteers during the hyperventilation challenge.

Volunteer no.	Model	$\Delta D/D$ (%)	$\Delta K/K$ (%)
1	Biexp-IVIM	7.7	
	DKI–IVIM	18.5	17.6
2	Biexp-IVIM	−6.9	
	DKI–IVIM	−8.7	7.8
3	Biexp-IVIM	2.0	
	DKI–IVIM	1.6	−4.7
4	Biexp-IVIM	1.6	
	DKI–IVIM	−2.4	−6.8
5	Biexp-IVIM	3.0	
	DKI–IVIM	14.9	16.5
6	Biexp-IVIM	−1.8	
	DKI–IVIM	2.8	13.0
7	Biexp-IVIM	−1.8	
	DKI–IVIM	−1.3	0.8
8	Biexp-IVIM	−5.3	
	DKI–IVIM	1.3	19.4

Table 4. Individual normalized percent changes of the IVIM diffusion parameter D (for the bi-exponential IVIM model) and D and K (for the DKI-IVIM model) in the cerebellum gray matter ROI, from the 8 healthy volunteers during the hyperventilation challenge.